



This is a repository copy of *Experimental observations on the influence of hydrogen atoms diffusion on laminar and turbulent premixed burning velocities.*

White Rose Research Online URL for this paper:  
<http://eprints.whiterose.ac.uk/110183/>

Version: Accepted Version

---

**Article:**

Burluka, A.A., Gaughan, R.G., Griffiths, J.F. et al. (3 more authors) (2017) Experimental observations on the influence of hydrogen atoms diffusion on laminar and turbulent premixed burning velocities. *Fuel*, 189. pp. 66-78. ISSN 0016-2361

<https://doi.org/10.1016/j.fuel.2016.10.088>

---

Article available under the terms of the CC-BY-NC-ND licence  
(<https://creativecommons.org/licenses/by-nc-nd/4.0/>)

**Reuse**

This article is distributed under the terms of the Creative Commons Attribution-NonCommercial-NoDerivs (CC BY-NC-ND) licence. This licence only allows you to download this work and share it with others as long as you credit the authors, but you can't change the article in any way or use it commercially. More information and the full terms of the licence here: <https://creativecommons.org/licenses/>

**Takedown**

If you consider content in White Rose Research Online to be in breach of UK law, please notify us by emailing [eprints@whiterose.ac.uk](mailto:eprints@whiterose.ac.uk) including the URL of the record and the reason for the withdrawal request.



[eprints@whiterose.ac.uk](mailto:eprints@whiterose.ac.uk)  
<https://eprints.whiterose.ac.uk/>

1 **Experimental Observations on the Influence of**  
2 **Hydrogen Atoms Diffusion on Laminar and**  
3 **Turbulent Premixed Burning Velocities**

4 A.A. Burluka<sup>a</sup>, R.G. Gaughan<sup>b</sup>, J.F. Griffiths<sup>c</sup>, C. Mandilas<sup>a,\*</sup>, C.G.W. Sheppard<sup>a</sup>, R. Woolley<sup>d</sup>

5  
6 <sup>a</sup> School of Mechanical Engineering, The University of Leeds, Leeds LS2 9JT, UK

7  
8 <sup>b</sup> ExxonMobil Research and Engineering Company, Paulsboro Technical Center, 600 Billingsport  
9 Road, Paulsboro, NJ 08066, USA

10  
11 <sup>c</sup> School of Chemistry, The University of Leeds, Leeds, LS2 9JT, UK

12  
13 <sup>d</sup> The University of Sheffield, Department of Mechanical Engineering, Mappin Street, S1 3JD,  
14 UK

15  
16 <sup>\*</sup> Corresponding author. Present address: The Centre for Research and Technology, Hellas,  
17 Chemical Process & Energy Resources Institute, 3km Charilaou-Thermi Road, Thermi 57001,  
18 Greece, mandilas@cperi.certh.gr

19  
20

21 **Abstract**

22 Measurements of the laminar and turbulent burning velocity of premixed hydrogen – air, n-  
23 hexane – air and n-octane – air flames were made and compared to corresponding measurements  
24 of deuterium – air, n-hexane-d14 – air and n-octane-d18 – air flames performed at identical initial  
25 conditions. Experiments were conducted in a constant volume, optically accessed vessel, at  
26 elevated initial pressure and temperature of 0.5 MPa and 360 K, for a range of equivalence ratios.  
27 Burn rate data was determined via schlieren imaging of flames. It was found that the isotope  
28 effect accounted for an average reduction of 20% in the laminar burn rate of alkanes. Similarly,  
29 deuterium was measured to burn around 30% slower than hydrogen at the range of equivalence  
30 ratios explored. The isotope effect on burn rate was significantly reduced under turbulence. The  
31 difference between the turbulent burn rates of the deuterated alkanes and their normal alkane  
32 counterparts were measured to be approximately 10%. The difference between the turbulent burn  
33 rates of deuterium and hydrogen was even smaller. Nonetheless, the laminar burn rate ranking  
34 was maintained under turbulence for all fuels and conditions explored, thus suggesting a degree  
35 of influence of radical transport and chemistry under turbulent burning.

36  
37 Keywords: laminar flames, turbulent flames, burning velocity, hydrogen combustion, deuterium  
38 combustion, isotope effect

39  
40 **Nomenclature**

41 Latin Symbols

42	D	$\text{m}^2/\text{s}$	Mass diffusivity
43	k	$\text{m}^3/\text{mol.s}$	Reaction rate coefficient

44	$L$	m	Integral length scale of turbulence
45	$L_b$	m	Burnt Markstein length
46	$P_i$	Pa	Initial pressure
47	$r_u$	m	Cold flame mean flame radius
48	$T_{ad}$	K	Adiabatic flame temperature
49	$T_i$	K	Initial temperature
50	$S$	-	Laminar burning velocity sensitivity factor
51	$u'$	m/s	Turbulent root-mean-square velocity
52	$u_l$	m/s	Unstretched, one-dimensional laminar burning velocity
53	$u_n$	m/s	Stretched, entrainment laminar burning velocity
54	$u_{te}$	m/s	Entrainment turbulent burning velocity

55

56 Greek Symbols

57	$\alpha$	$m^2/s$	Thermal diffusivity
58	$\alpha_{mix}$	$m^2/s$	Thermal diffusivity of mixture
59	$\alpha$	1/s	Flame stretch rate
60	$\delta_l$	m	Laminar flame thickness
61	$\eta$	m	Kolmogorov length scale of turbulence
62	$\phi$	-	Equivalence ratio
63	$\omega$	$(m^3/mol.s)^n$	Global reaction rate

64

65 **1. Introduction**

66 The molecular structure of a fuel (i.e. length of chain, branching, bonding) is known to greatly  
67 influence the laminar burn rate [1-5]. Fuel structure in conjunction with mixture stoichiometry,  
68 pressure and temperature, govern the thermodynamics and chemical kinetics of combustion. One  
69 of the main driving forces of chemical kinetic contributions to the control of burning velocity is  
70 the radical pool at the flame front, with H atoms being the most important by virtue of their  
71 extremely high diffusivity and reactivity [4-5].

72 In two previous papers we investigated the effects of fuel structure on the laminar and turbulent  
73 burning velocities of gasoline components. We assessed:

74 (i) isomeric structure and bonding through experimental studies of seven different hydrocarbons  
75 containing six carbon atoms, over a wide range of fuel - air mixtures [6] and

76 (ii) chain length and molecular mass by reference to straight chain alkanes in the range  $C_5 - C_8$   
77 [7].

78 Interpretation of the results was linked to the influence of H radicals at the flame front in  
79 controlling the burn rate.

80 The object of the present work was to understand the importance of the transport and kinetic  
81 effects of hydrogen radicals within laminar and turbulent premixed flames via experimental  
82 studies of burning velocity measurements of freely propagating flames. Hence, we have extended  
83 the earlier studies [6, 7] through comparisons of laminar and turbulent velocity of n-hexane and  
84 n-octane (i.e.  $n-C_6H_{14}$  and  $n-C_8H_{18}$ ) with those of their fully deuterated forms (i.e.  $n-C_6D_{14}$  and  $n-$   
85  $C_8D_{18}$ ). In interpretation of the results, it is assumed that there are no qualitative differences in the  
86 kinetic mechanisms involved in flame propagation of the normal and deuterated fuels. In

87 addition, we explore the H / D isotopic effect in its most influential guise, via an investigation of  
88 the laminar and turbulent burning velocities of H<sub>2</sub> and D<sub>2</sub>.  
89 The available literature on the isotopomeric effects in combustion is sparse. With the exception  
90 of a study of laminar flame propagation in acetylene and di-deuteroacetylene by Friedman and  
91 Burke [8], we are not aware of any other investigation of the laminar and turbulent burn rates of  
92 deuterated versus normal hydrocarbons, even though the former are occasionally used for tracing  
93 the origins of pollutants in flames, e.g. [9]. Moreover, although hydrogen burn rate data exist for  
94 a variety of conditions [e.g. 10-18] there is only very little information on the laminar burn rates  
95 of D<sub>2</sub> [19-21] and, to our knowledge, no comparisons between the turbulent burn rates of H<sub>2</sub>-air  
96 and D<sub>2</sub>-air flames.

97

## 98 **2. Experimental Apparatus and Data Processing**

99 All measurements were performed in the Leeds MkII spherical bomb [22]. As in the previous  
100 studies for the examination of fuel structure and chain length effects on burn rate [6-7],  
101 measurements were performed at elevated temperature and pressure (360 K and 0.5 MPa), at  
102 which the premixed turbulent flames demonstrate behaviour similar to flames in spark-ignition  
103 engines [22]. Owing to the high cost of the deuterated fuels, the alkane tests were undertaken at  
104 only  $\phi = 0.8$  and  $\phi = 1.0$  for laminar conditions and at  $\phi = 1.0$  under turbulent conditions. For the  
105 latter, the turbulence level was set at an rms velocity of  $u' = 4$  m/s. The burn rates of H<sub>2</sub> and D<sub>2</sub>  
106 were examined for laminar and turbulent ( $u' = 4$  m/s) conditions for  $0.6 \leq \phi \leq 1.1$ . The turbulence  
107 rms velocity of  $u' = 4$  m/s chosen for this study was relevant to reciprocating engines, where  $u'$   
108 near the top dead centre is about half the piston speed (e.g.  $u' = 5$  m/s, for 75 mm stroke, at 4000  
109 rpm [23]).

110 Premixed mixtures were prepared inside the fan-stirred vessel. Pre-calculated volumes of liquid  
111 fuels were injected into the vessel under vacuum conditions, using a gas tight syringe. For  
112 gaseous fuels, the mixture stoichiometry was controlled by measuring the partial pressure of the  
113 fuel injected into the bomb at atmospheric pressure. The bomb fans were continuously operated  
114 during mixture preparation to ensure full mixing and to assist heat transfer from the 2 kW  
115 electrical heater, positioned close to the walls of the vessel. For laminar studies, the fans were  
116 switched off for a period of 60 seconds, following mixture preparation, and before ignition. For  
117 turbulent studies the fans were maintained at the speed required to produce the desired rms  
118 turbulent velocity throughout the mixture preparation, ignition and combustion period. The  
119 pressure in the vessel before ignition was measured via an absolute pressure transducer (Druck  
120 PDCR-911) with a range of 0 to 0.7 MPa. Following spark discharge, the pressure rise in the  
121 vessel was monitored with a Kistler-701 piezoelectric pressure transducer, flush mounted on the  
122 side of the vessel. After each experiment the vessel was flushed several times with compressed  
123 air and then evacuated. Dry cylinder air was provided for the combustible mixture.

124 At least two laminar and five turbulent deflagrations were performed at each condition. Centrally  
125 ignited advancing flames were imaged via the schlieren method to the bomb window diameter of  
126 150 mm, using a Photsonics Phantom Series 9 high speed digital camera. Laminar flames were  
127 recorded at 4000 frames/s with a resolution of 576x576 pixels. Turbulent flames were  
128 photographed at a rate of 9000 frames/s with a resolution of 384x384 pixels.

129 During post-processing of schlieren data, each flame image was converted from grayscale to  
130 black and white. White corresponded to the burned and black to the unburned region. The flame  
131 area was found by counting the number of white pixels. The burning velocity was then defined as  
132 the radius derivative with respect to time divided by the ratio of densities of the fresh mixture to

133 that of the combustion products. Mean flame radius was determined as that of a circle  
134 encompassing the same area. Further information on the flame image processing procedure is  
135 given in [6, 24]. Imaging data analysis to obtain laminar flame characteristics (burning velocity,  
136 stretch rate and Markstein lengths) and turbulent burn rates followed established methods,  
137 detailed [25-26] and widely used elsewhere [eg. 27-31].

138

### 139 **3. Results**

140 Presented in this section are measured laminar and turbulent burn rate results for normal and  
141 deuterated alkanes, hydrogen and deuterium. Experimental scatter for laminar deflagrations was  
142 at a maximum of 2% with respect to the coefficient of variance (COV) of the laminar burning  
143 velocity at any given flame radius. Turbulent deflagrations reported here exhibited an average  
144 scatter of circa 7-8% in COV of the turbulent burn rate at a given flame radius, which was similar  
145 to that reported in [32] and is typical of the magnitude of cycle-to-cycle variation of the burning  
146 rate in an SI engine [33].

147 In addition to data for the unstretched, one dimensional, laminar burning velocity,  $u_l$ , derived in  
148 accord with [26], the laminar results for the alkanes also include data for the stretched laminar  
149 burning velocities,  $u_n$ , at mean flame radii of 10 mm and 30 mm. Due to the comparable molar  
150 mass of n-hexane versus n-hexane-d14 and n-octane versus n-octane-d18, stretch rate effects  
151 were anticipated to be similar and, therefore, to not affect the trends observed for the laminar  
152 burn rate ratio of normal vs deuterated alkanes.

153 For  $H_2$  and  $D_2$  laminar deflagrations, hydrodynamic flame instabilities [34-35] occurred too early  
154 to apply the criteria for unstretched laminar burning velocity [26]. It was thus decided to present



155 the schlieren-derived stretched burning velocities at mean flame radii of 10 mm and 30 mm to  
156 allow comparison to previous studies [13] and ensure exclusion of spark effects [36].

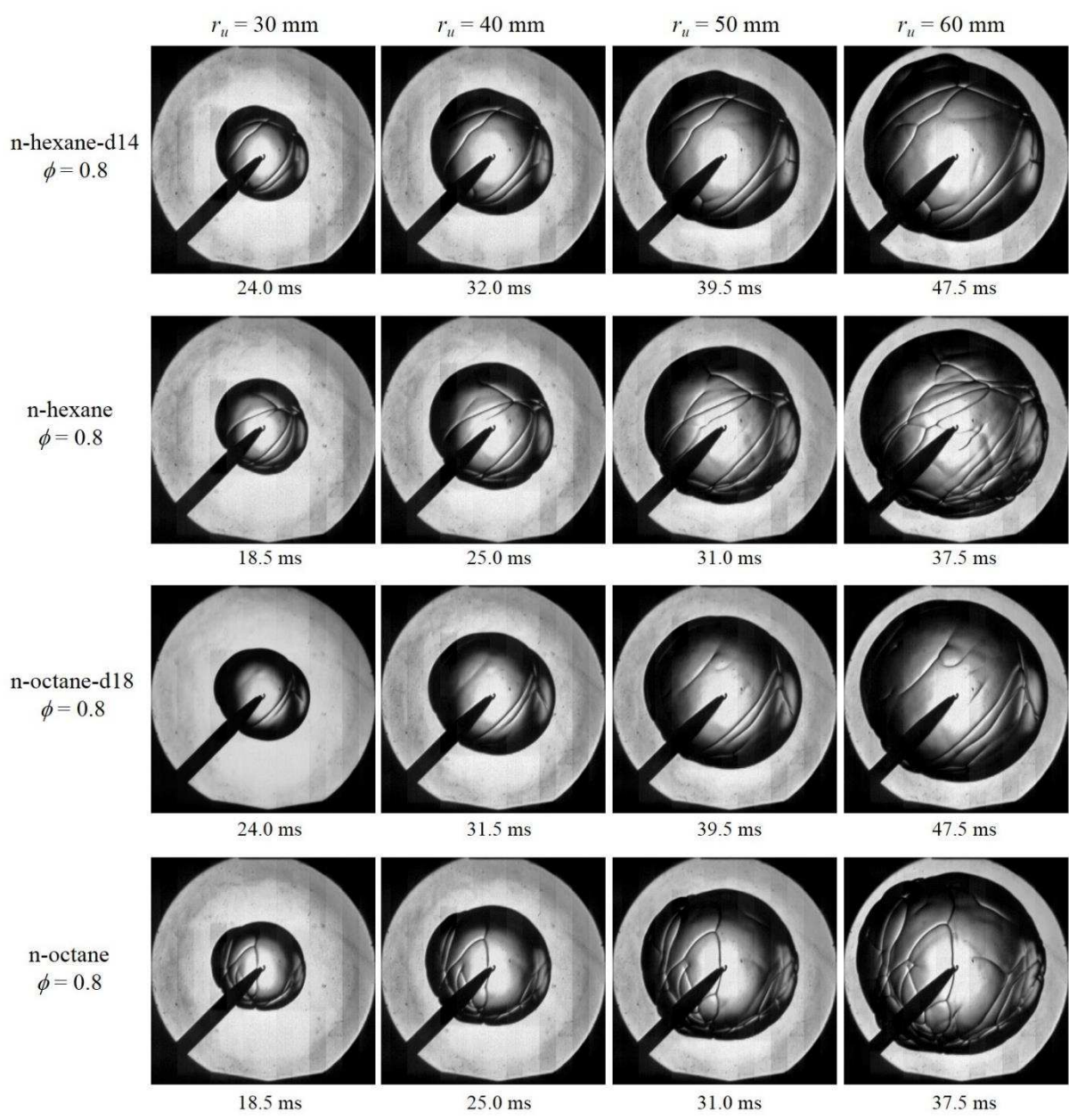
157 All schlieren based turbulent burn rates,  $u_{te}$ , refer to a mean flame radius of 30 mm. Reasons  
158 behind this choice are discussed in [6]. As a brief recapitulation here, presentation of the  
159 turbulent burn rate results at this radius offered the best compromise between ensuring that the  
160 flame had experienced most (~ 62% [25]) of the effective turbulence [37] inside the vessel, while  
161 also avoiding extra difficulties during image processing induced due to flame convection from  
162 the centre of the visible area of the vessel, which is a particular problem for lean, high turbulence  
163 flames [24].

164

### 165 **3.1 Laminar Burning Velocities of the Alkanes**

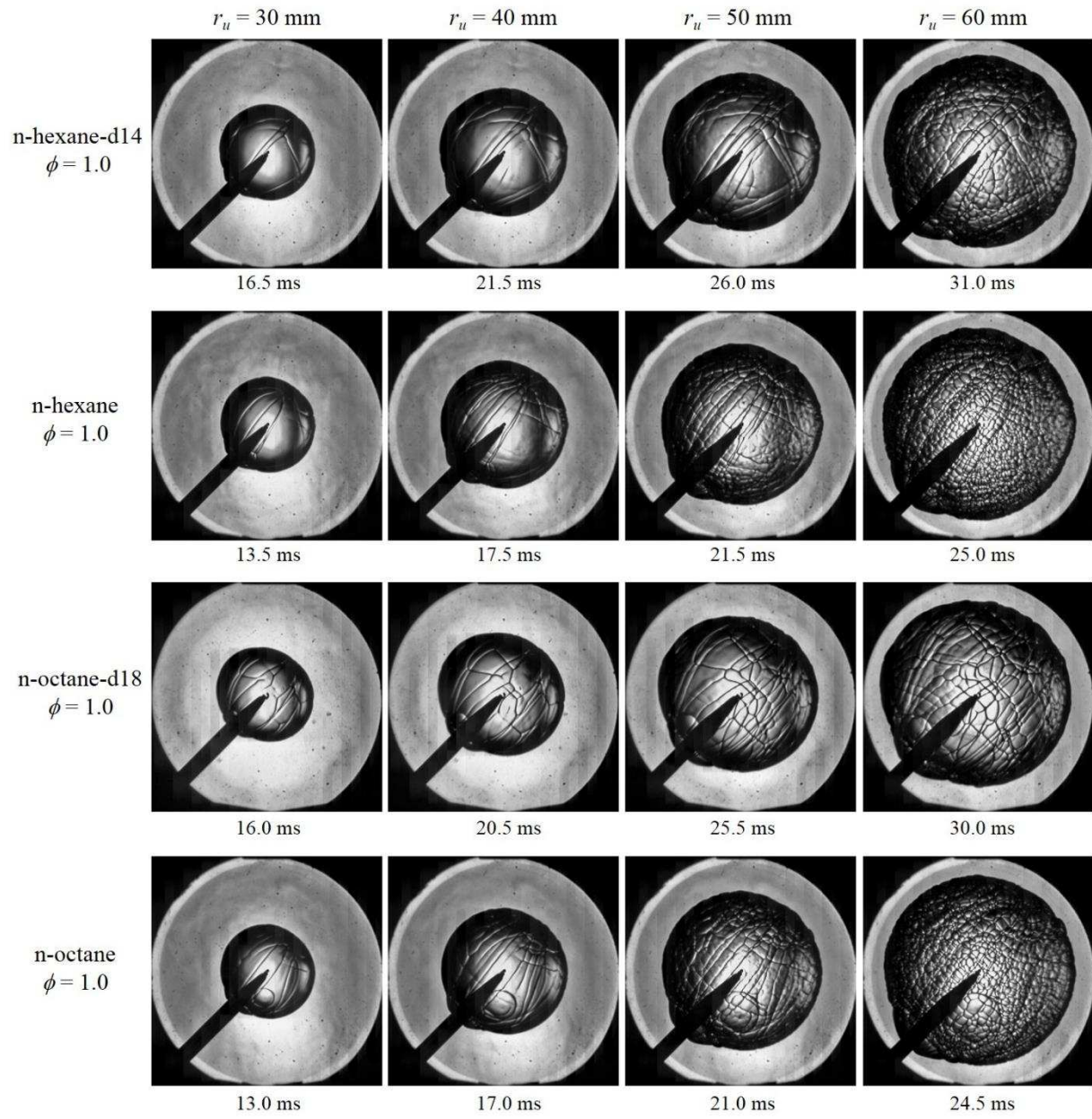
166 The development of spherical expanding flames of normal and deuterated hexane and octane is  
167 depicted via the sequences of schlieren images displayed in Figure 1 for  $\phi = 0.8$  and Figure 2 for  
168  $\phi = 1.0$ . Starting at mean flame radii of 30 mm, the images of each of the flame filmstrips are in  
169 steps of  $10 \pm 0.2$  mm in mean flame radius. Also shown below each image is the time elapsed  
170 from the first visible flame kernel following ignition. Although lean flames did not exhibit  
171 transition to fully cellular structure within the field of view of the bomb windows, the formation  
172 of large scale cells on the flame surface was more apparent for the normal than for the deuterated  
173 alkanes at radii of  $60 \pm 0.2$  mm. Flames at stoichiometric conditions became fully cellular at ca.  
174 45 mm for the normal alkanes and at ca. 50 mm for the deuterated alkanes. This is linked to  
175 differences in the thermo-diffusive properties at the flame front [35, 38], which in this case have  
176 been induced solely by the isotope effect. Note that the definition of the onset of cellularity was  
177 based on photographic observations for the formation of small scale cells at the flame surface

178 (Figures 1 and 2) in conjunction with identification of the point at which an appreciable flame  
 179 acceleration appears on the plot of burning velocity vs. mean flame radius, as described in [7,  
 180 35].  
 181



183 Figure 1 – Filmstrip (left to right) of schlieren images showing the flame development for normal  
 184 and deuterated alkane flames of  $\phi = 0.8$ . The mean flame radius values indicated have an  
 185 accuracy of  $\pm 0.2$  mm, while the time values shown in milliseconds represent time elapsed from  
 186 the first visible flame kernel following ignition.

187

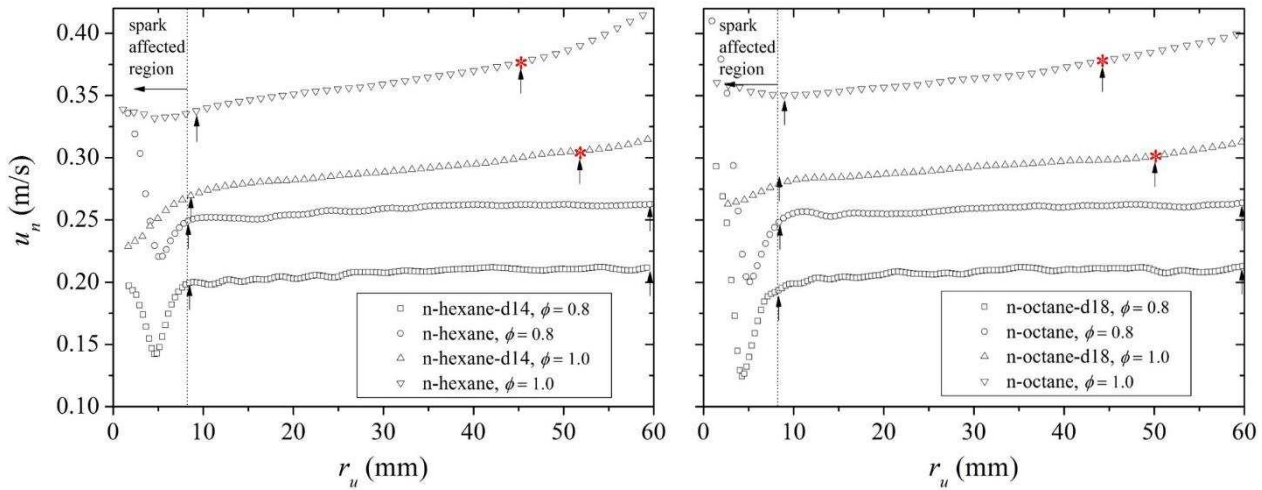


188

189 Figure 2 – Filmstrip (left to right) of schlieren images showing the flame development for normal  
190 and deuterated alkane flames of  $\phi = 1.0$ . The mean flame radius values indicated have an  
191 accuracy of  $\pm 0.2$  mm, while the time values shown in milliseconds represent time elapsed from  
192 the first visible flame kernel following ignition.

193  
194

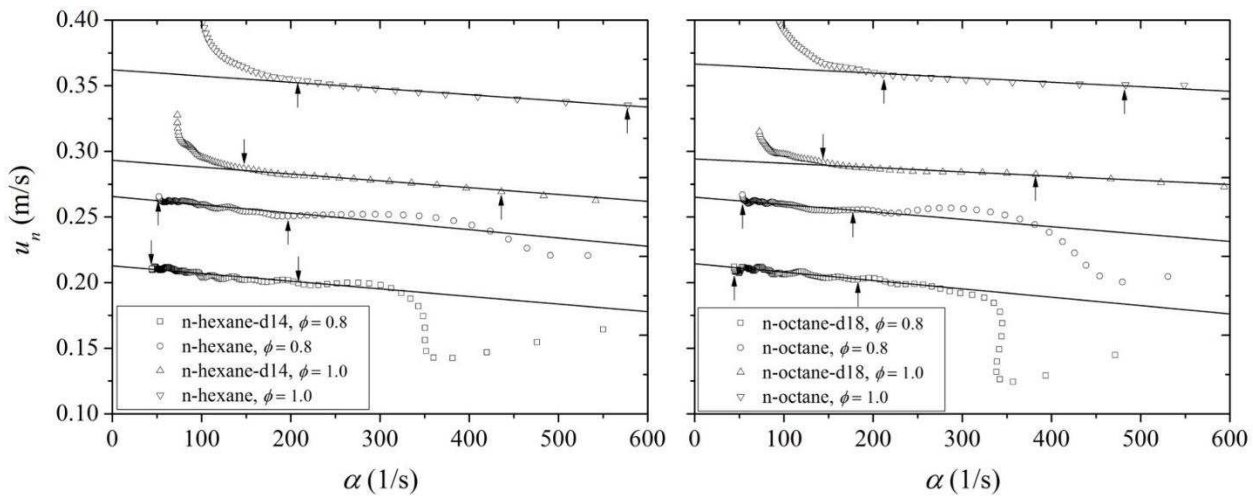
195 The onset of apparent transition to fully cellular flames is specified on the  $u_n$  vs  $r_u$  plots of Figure  
196 3 via the red asterisk symbols on top of the data points. Also specified on these plots is the early  
197 flame development region affected by the characteristics of the igniter. Spark energy much above  
198 the minimum ignition energy, can cause a very high initial flame speed due to the expansion of  
199 the plasma and the conductive energy transfer from it; these data are disregarded [26]. Previous  
200 measurements in the same apparatus have shown the spark affected area to be up to a mean flame  
201 radius of 8-10 mm [36]. For lean flames the slight increase in burning velocity with radius is  
202 attributed to the reduction of stretch rate with flame radius, as well as to a small increase of  $\sim 10$   
203 K in unburned gas temperature over that period of flame development [24]. Stoichiometric  
204 flames exhibited similar behaviour up to the point of transition to fully cellular regime, upon  
205 which a slight increase in flame acceleration was observed, for reasons described in [7]. For  
206 completion, the variation of burning velocity with stretch rate ( $\alpha$ ) is shown in Figure 4, along  
207 with the range of data over which the laminar flame theory described in [26] was applied to  
208 determine the true laminar, one-dimensional and unstretched burning velocities,  $u_1$ .



209

210 Figure 3 – Stretched burning velocity,  $u_n$ , plotted against mean flame radius,  $r_u$ , for normal and  
 211 deuterated alkanes at  $\phi = 0.8$  and 1.0. Vertical arrows indicate the data regions used for  
 212 application of laminar burn rate theory to obtain unstretched burning velocity and Markstein  
 213 lengths. The red asterisks indicate the onset of transition to fully cellular regime.

214



215

216 Figure 4 – Variation of stretched burning velocity,  $u_n$ , with stretch rate,  $\alpha$ , for the normal and  
 217 deuterated alkanes at  $\phi = 0.8$  and 1.0. Vertical arrows indicate the data regions used for  
 218 application of laminar burn rate theory to obtain unstretched burning velocity and Markstein  
 219 lengths

220

221 Data for  $u_l$ ,  $u_{n,10mm}$  and  $u_{n,30mm}$  are presented in tabulated form in Tables 1 for  $\phi = 0.8$  and Table 2  
 222 for  $\phi = 1.0$ . The deuterated alkanes were found to burn approximately 20% slower than their  
 223 normal alkane counterparts, a proportion that was independent of equivalence ratio, flame radius  
 224 or whether the flame was unstretched or stretched.

	n-C <sub>6</sub> H <sub>14</sub> (m/s)	n-C <sub>6</sub> D <sub>14</sub> (m/s)	$u_{C_6D_{14}} /$ $u_{C_6H_{14}}$	n-C <sub>8</sub> H <sub>18</sub> (m/s)	n-C <sub>8</sub> D <sub>18</sub> (m/s)	$u_{C_8D_{18}} /$ $u_{C_6H_{18}}$
$u_l$	0.266 ± 0.001	0.214 ± 0.002	0.805	0.265 ± 0.001	0.214 ± 0.001	0.808
$u_{n,10mm}$	0.253 ± 0.002	0.202 ± 0.005	0.798	0.251 ± 0.007	0.198 ± 0.001	0.789
$u_{n,30mm}$	0.260 ± 0.001	0.212 ± 0.006	0.814	0.258 ± 0.002	0.208 ± 0.001	0.806

225  
 226 Table 1 – Measured average laminar burning velocities for normal and deuterated alkanes at  $\phi =$   
 227 0.8, with  $T_i = 360$  K and  $P_i = 0.5$  MPa. Also included are the standard deviation of the measured  
 228 values and the ratios of the measured burn rates of deuterated over normal alkanes.

229

	n-C <sub>6</sub> H <sub>14</sub> (m/s)	n-C <sub>6</sub> D <sub>14</sub> (m/s)	$u_{C_6D_{14}} /$ $u_{C_6H_{14}}$	n-C <sub>8</sub> H <sub>18</sub> (m/s)	n-C <sub>8</sub> D <sub>18</sub> (m/s)	$u_{C_8D_{18}} /$ $u_{C_6H_{18}}$
$u_l$	0.366 ± 0.005	0.292 ± 0.003	0.798	0.364 ± 0.003	0.294 ± 0.004	0.807
$u_{n,10mm}$	0.343 ± 0.005	0.274 ± 0.002	0.799	0.346 ± 0.005	0.281 ± 0.001	0.812
$u_{n,30mm}$	0.361 ± 0.001	0.288 ± 0.003	0.798	0.362 ± 0.003	0.293 ± 0.002	0.809

230  
 231 Table 2 – Measured average laminar burning velocities for normal and deuterated alkanes at  $\phi =$   
 232 1.0, with  $T_i = 360$  K and  $P_i = 0.5$  MPa. Also included are the standard deviation of the measured  
 233 values and the ratios of the measured burn rates of deuterated over normal alkanes.

234

235 The burned gas Markstein length,  $L_b$ , is a physico-chemical flame parameter used to characterise  
 236 the effect of stretch rate on burn rate [35]. A small value of  $L_b$  is indicative of small influence of

237 flame stretch rate on burning velocity [26]. Burned gas Markstein lengths were determined as the  
 238 slope of the linear fits in the  $u_n$  vs  $\alpha$  plots (Figure 4). It should be noted that compared to the  
 239 linear stretch corrections employed here, application of non-linear stretch corrections for the  
 240 same data led to differences smaller than the experimental accuracy. Average  $L_b$  results for the  
 241 conditions explored here are shown in Table 3 and demonstrate great similarity between the  
 242 normal and deuterated alkanes, hence supporting the interpretation that the difference in burning  
 243 velocity was independent of flame stretch (i.e. as shown in Tables 1 and 2). The similarity in  $L_b$   
 244 between the alkanes examined is likely to be due to their similar molar masses.

245

	n-C <sub>6</sub> H <sub>12</sub> , L <sub>b</sub> (mm)	n-C <sub>6</sub> D <sub>12</sub> , L <sub>b</sub> (mm)	n-C <sub>8</sub> H <sub>16</sub> , L <sub>b</sub> (mm)	n-C <sub>8</sub> D <sub>16</sub> , L <sub>b</sub> (mm)
$\phi = 0.8$	0.37 ± 0.020	0.37 ± 0.019	0.38 ± 0.049	0.39 ± 0.009
$\phi = 1.0$	0.33 ± 0.004	0.32 ± 0.012	0.27 ± 0.025	0.23 ± 0.044

246

247 Table 3 – Measured average Markstein lengths,  $L_b$ , for the normal and deuterated alkanes. Also  
 248 included is the standard deviation between measurements performed at given equivalence ratios.

249

250 Normal versus deuterated alkanes have no differences in molecular structure and equilibrium  
 251 calculations revealed negligible differences in adiabatic flame temperature,  $T_{ad}$ . Likewise,  
 252 computations suggested very similar thermal and mass diffusion coefficients for these fuel-air  
 253 mixtures (Table 4). The estimates displayed in Table 4 were based on the kinetic theory of gases  
 254 developed by Chapman and Enskog and described in detail in [39], in conjunction with multi-  
 255 component transport coefficients derived with the use of the equations defined in [40]. The  
 256 thermodynamic data required for the calculations were provided by ExxonMobil [41]. Collision  
 257 radii and reduced energies for the application of the kinetic theory of gases were estimated from



258 critical temperature and pressure data found in the NIST online library [42]. It may thus be  
 259 concluded that since the values of thermal and mass diffusivity of the deuterated and normal  
 260 alkane-air mixtures are virtually identical, the observed difference in burning velocities cannot be  
 261 attributed to transport properties of the fuel molecule.

Temperature, T	$\frac{a_{C_6D_{14}\text{-air}}}{a_{C_6H_{14}\text{-air}}}$	$\frac{a_{C_8D_{18}\text{-air}}}{a_{C_8H_{18}\text{-air}}}$	$\frac{D_{C_6D_{14}\text{-air}}}{D_{C_6H_{14}\text{-air}}}$	$\frac{D_{C_8D_{18}\text{-air}}}{D_{C_8H_{18}\text{-air}}}$
360 K	0.995	0.997	0.973	0.977
$T = T_{ad} \approx 2350$ K	1.000	0.999	0.974	0.978

262  
 263 Table 4 – Ratios of thermal,  $\alpha$ , and mass, D, diffusivities of deuterated versus normal alkane-air  
 264 stoichiometric mixtures at 360 K and  $T = T_{ad}$ , at constant pressure of 0.5 MPa.

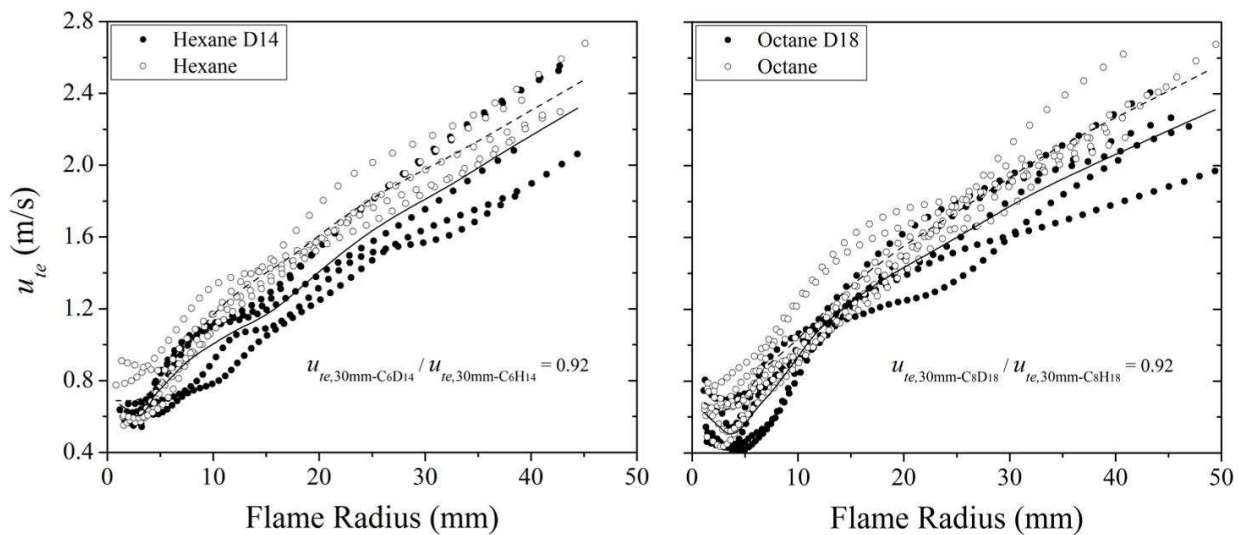
265  
 266 To put the reduction of the laminar burning velocity of the deuterated alkanes relative to their  
 267 respective hydrogen-containing counterparts in perspective, it was recently shown [6] that for  
 268 identical conditions ( $T_i$ ,  $P_i$ ,  $\phi$ ), the unstretched burning velocity of the hexane isomer, 2,2-  
 269 dimethyl butane, was measured to be 15% lower than that of n-hexane. This difference may be  
 270 attributed to (i) the potential for the production of a higher proportion of  $CH_3$  radicals during  
 271 branched alkane combustion relative to those generated during n-alkane combustion, and (ii) the  
 272 predominance of primary C-H bonds relative to the number of secondary C-H bonds in the n-  
 273 alkane [4, 6]. Any causes of the 20% difference measured here between n-hexane and n-hexane-  
 274 d14 pertaining to chemistry are limited to kinetic isotope effects of reaction rates involving H  
 275 versus D atoms derived from the primary fuel molecule or contained in other combustion  
 276 intermediates. However, a very important, supplementary factor which also affects laminar flame  
 277 propagation is the lower diffusivity of D versus H atoms.

278

### 279 3.2 Turbulent Burning Velocities of the Alkanes



280 Turbulent tests were performed solely at  $\phi = 1.0$  for a turbulent r.m.s. velocity of 4 m/s. Schlieren  
 281 derived turbulent burn rates plotted against flame radius are shown in Figure 5. The reasoning  
 282 behind setting 30 mm as the reference mean flame radius was explained at the beginning of  
 283 Section 3. It was found that the deuterated fuels remained slower than their conventional  
 284 counterparts under turbulence. However, the differences were substantially reduced compared to  
 285 the laminar flames. Nevertheless, overall reductions throughout flame development subsequent to  
 286 the spark affected region remained at 5-10% as a result of the substitution of H for D in both of  
 287 the alkanes that were studied here. The average difference in burn rate between normal and  
 288 deuterated alkanes at the reference radius of 30 mm was 8% (Figure 5).



289  
 290 Figure 5 – Turbulent burning velocities ( $u' = 4$  m/s) for the alkanes plotted against mean flame  
 291 radius. The curves in the plots are averages at set radii obtained via linear interpolation; dashed  
 292 lines for normal alkanes, solid lines for deuterated alkanes. Also shown are ratios of the normal  
 293 vs. deuterated alkane at the reference radius of 30 mm.

294  
 295 A similar reduction of the differences between the burn rates of various hydrocarbon fuels when  
 296 moving from laminar to turbulent conditions was reported in the previous paper [6] of the overall

297 study, which addressed the influence of molecular structure for a series of C<sub>6</sub> hydrocarbon fuels.  
298 As discussed in Section 3.1, the unstretched laminar burning velocity of 2,2 dimethyl butane has  
299 been found to be ~15% lower than that of n-hexane for near stoichiometric conditions, at 0.5 MPa  
300 and 360 K [6]. However, at the same equivalence ratio, pressure and temperature, the turbulent  
301 burning velocity of 2,2 dimethyl butane was only ~9% lower than that of n-hexane (at  $u' = 2$  m/s  
302 and 6 m/s). Similarly [6], at the same equivalence ratio, pressure and temperature conditions, 2-  
303 methyl pentane was measured to have ~11% lower laminar burn rate than n-hexane, whereas its  
304 turbulent burn rate was found to be ~5% slower than that of n-hexane at  $u' = 2$  m/s and 6 m/s.  
305 These observations indicate that there are residual kinetic and transport processes influencing  
306 turbulent combustion. In the case of the C<sub>6</sub> work reported in [6], the kinetic differences were  
307 primarily linked to the propensity of production of CH<sub>3</sub> vs C<sub>2</sub>H<sub>5</sub> radicals during the initial steps of  
308 fuel oxidation and, consequently, the availability of H radicals and the facilitation of branching  
309 reactions at the flame front. Likewise, in the current work, the relative differences between the  
310 turbulent burn rate of the normal and deuterated alkanes studied here point to a specific  
311 contribution to turbulent flame propagation of the kinetics and transport processes involving H  
312 and D atoms and related radicals, such as OH / OD or HO<sub>2</sub> / DO<sub>2</sub>.

313 Based on the turbulent regime theory [43], the alkane flames explored were classified as  
314 thickened flamelets, for which the Kolmogorov turbulent scale,  $\eta$ , is typically less than the  
315 laminar flame thickness,  $\delta_l$ , and hence turbulence can penetrate the flame and alter the transport  
316 and chemistry of species at the flame front. In this case, application of the Zimont submodel for  
317 turbulent burning velocity [44], which has been extensively discussed elsewhere [45], is valid.

318

$$u_{te} \sim u^{0.75} L^{0.25} u_l^{0.5} \alpha^{-0.25} \quad (1)$$

319 In this work,  $u'$ , the rms turbulent velocity, and  $L$ , the integral length scale of turbulence,  
320 remained constant for all flames. The reduced differences measured when moving from laminar  
321 to turbulent conditions were adequately replicated via application of Eq. (1). Utilising  $u_l$  and  $\alpha$   
322 data from Tables 2 and 4, it can be shown that the turbulent burn rate ratios of  $C_6D_{14} / C_6H_{14}$  and  
323  $C_8D_{18} / C_8H_{18}$  predicted via Eq. (1) are 0.898 and 0.899, i.e. very similar to those experimentally  
324 measured at 0.9 – 0.95 throughout flame development within the vicinity of the bomb windows.  
325 Application of Eq. (1) for the  $C_6$  hydrocarbon pairs can be shown to yield similarly good  
326 agreement between predictions and actual measurements. Therefore, it could be concluded that  
327 for fuels of similar molar mass, and consequently transport properties, the kinetic processes at the  
328 flame front only influence turbulent burning velocity indirectly, through the laminar burning  
329 velocity accordingly to Eq. (1).

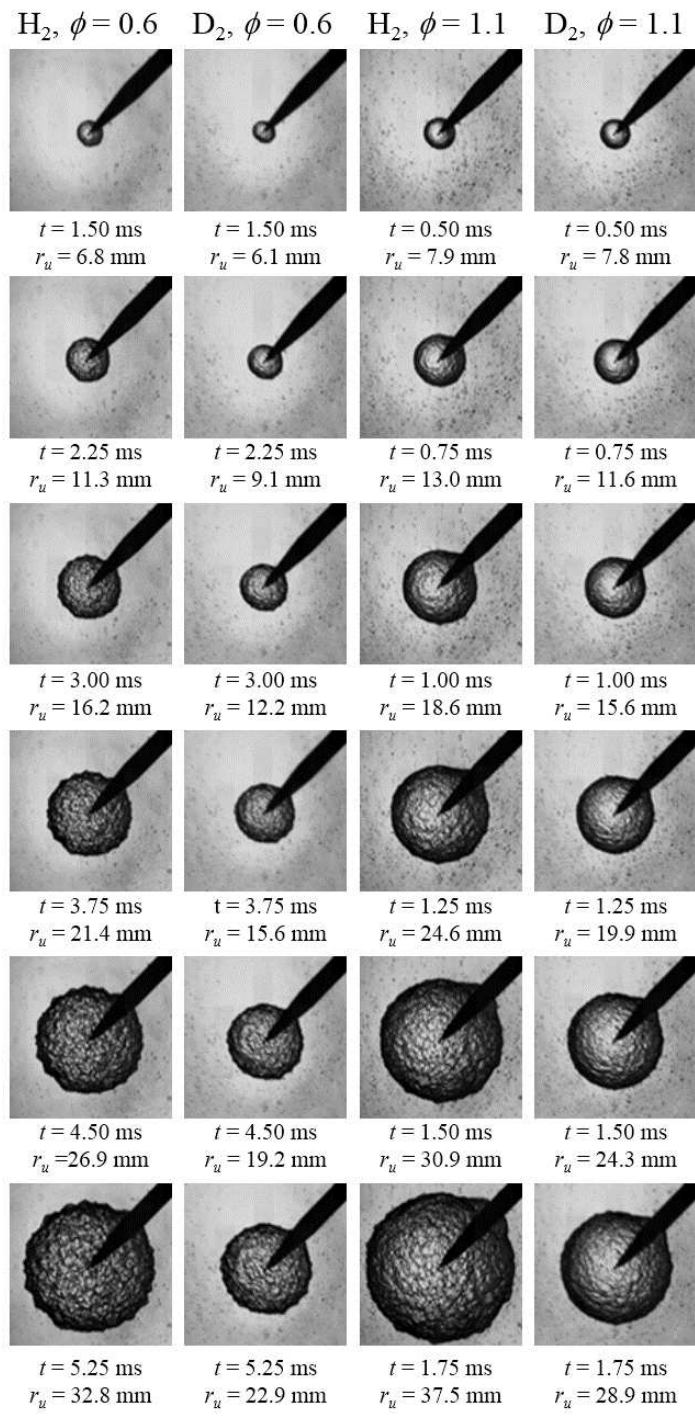
330

### 331 **3.3 Laminar Burning Velocities of $H_2$ and $D_2$**

332 The development of the leanest and richest hydrogen-air and deuterium-air flames examined in  
333 the current study is illustrated via the filmstrips of schlieren images shown in Figure 6. These  
334 images have been zoomed in to better demonstrate the extremely early transition to cellular  
335 regime almost immediately following ignition (i.e. at  $r_u < 10$  mm) for both fuels. To demonstrate  
336 the laminar flame development, shown in Figure 7 are plots of stretched laminar flame speed,  $u_n$ ,  
337 versus flame radius for the leanest and richest deuterium and hydrogen flames examined.

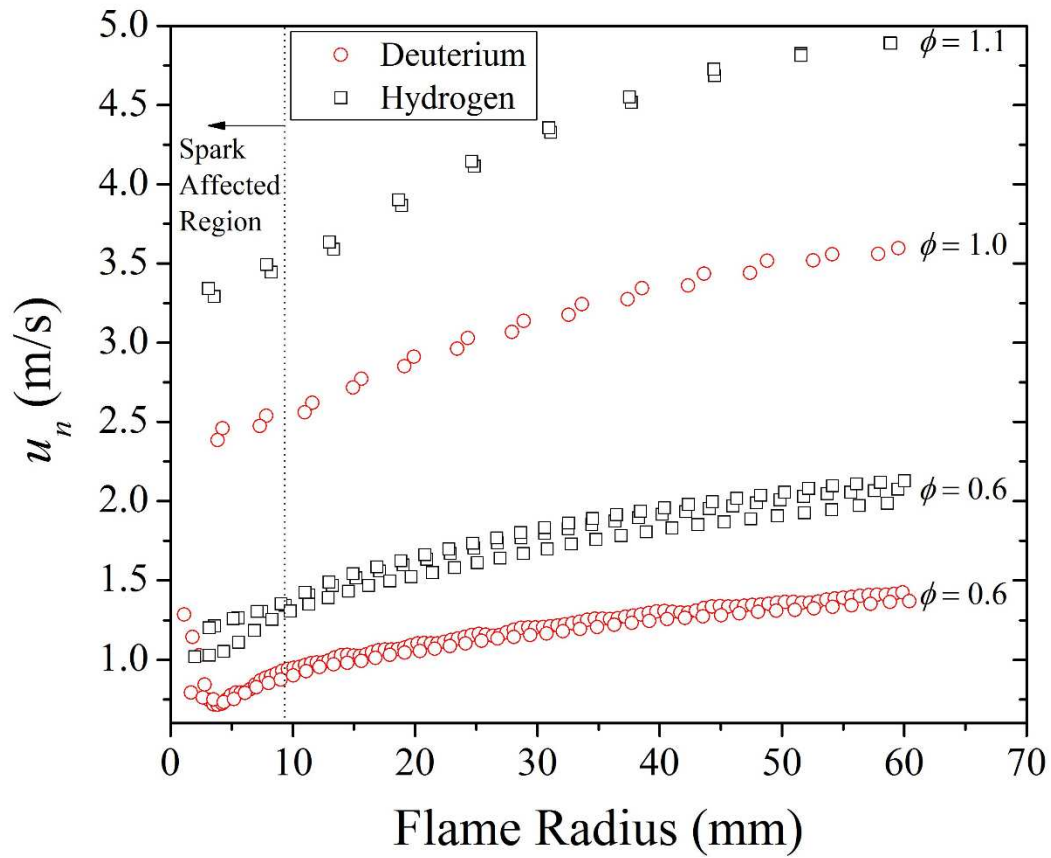
338 The results for the stretched laminar burning velocities,  $u_n$ , at mean flame radii of  $r_u = 10$  mm and  
339 30 mm are displayed in Figure 8. It is important to clarify that these burning velocities do not  
340 reflect the pure, one-dimensional, unstretched laminar burning velocity ( $u_l$ ). The reason is the  
341 extremely early transition of the  $H_2$  and  $D_2$  flames to a cellular regime, which made application of

342 the laminar flame theory to calculate  $u_1$  impossible [26]. Hence, in the case of the results of  
343 Figure 8, diffusion effects are twofold, as they also include the increased diffusivity arising from  
344 the increased surface area induced by cellularity. This effect is not expected to be identical  
345 between  $H_2$  and  $D_2$  flames. The propensity to cellularity in fuel-air flames is believed to be  
346 related to the Lewis number,  $Le = \alpha_{\text{mix}} / D_{\text{deficient reactant}}$ , of the deficient reactant [34].  
347 Computations following the methods described in [39] and [40] showed that at  $0.6 \leq \phi < 1.0$ ,  
348 where fuel is the deficient reactant, Lewis numbers for  $H_2$ -air flames were 20-25% smaller than  
349 those for  $D_2$ -air flames. Hence, instability effects are anticipated to be more prominent in  $H_2$  than  
350 in  $D_2$  at  $0.6 \leq \phi < 1.0$ .



351

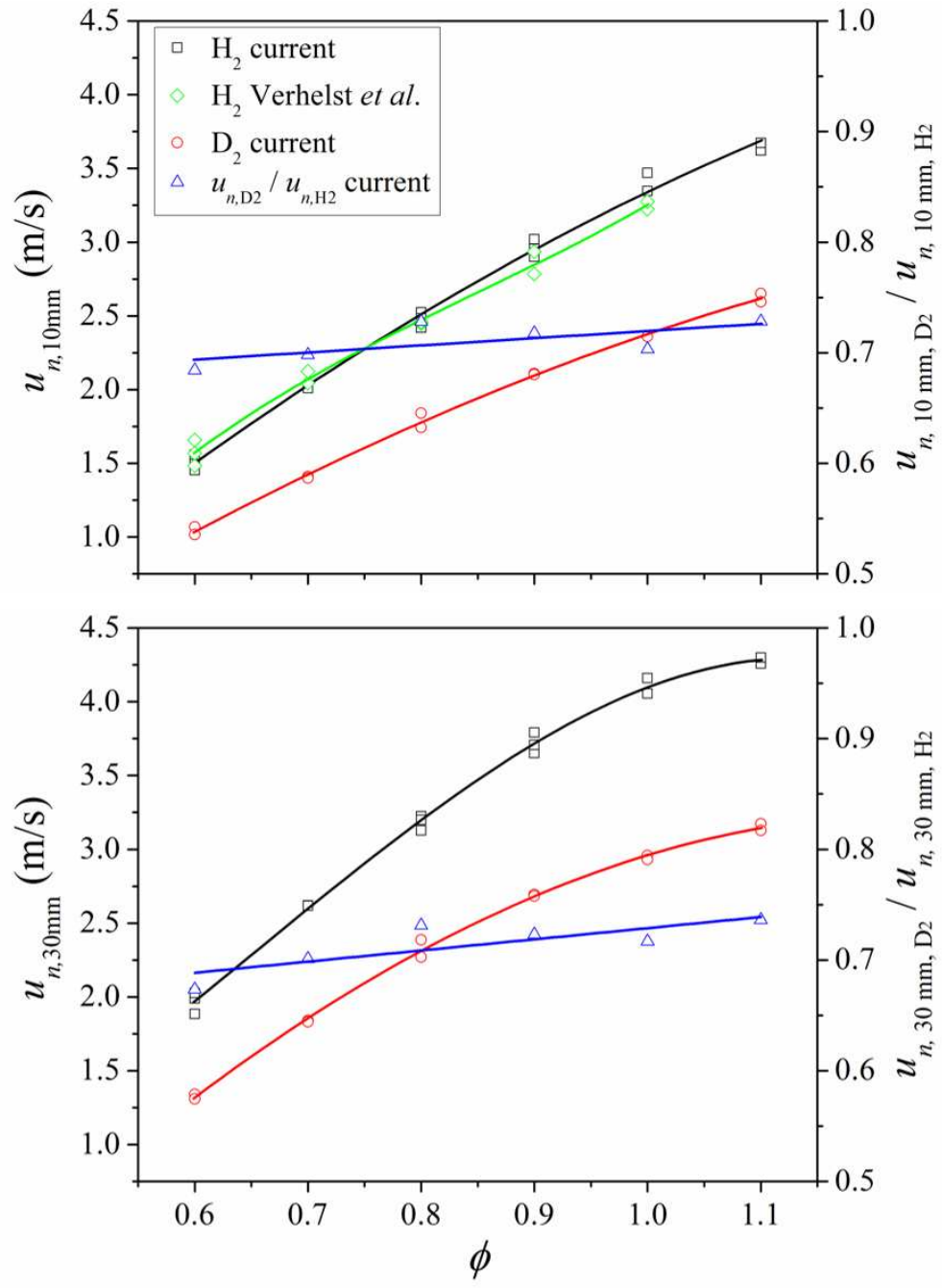
352 Figure 6 – Filmstrip (top to bottom) of schlieren images showing the flame development for  
 353 hydrogen-air and deuterium-air flames at  $\phi = 0.6$  and  $\phi = 1.1$ . The time values shown in ms  
 354 represent time elapsed from the first visible flame kernel following ignition.



355

356 Figure 7 – Plots of stretched burning velocity versus flame radius showing the flame  
 357 development of the leanest and richest hydrogen and deuterium flames studied.

358



359

360 Figure 8 – Schlieren based laminar burn rates for  $H_2$ -air,  $D_2$ -air flames at mean flame radii of 10  
 361 mm and 30 mm, plotted versus  $\phi$ . The curves are 3<sup>rd</sup> order polynomial fits of the experimental  
 362 data. Also included in the plot for mean flame radius of 10 mm (top) are data for the burn rate of  
 363  $H_2$  reported in [13] at identical conditions.

364

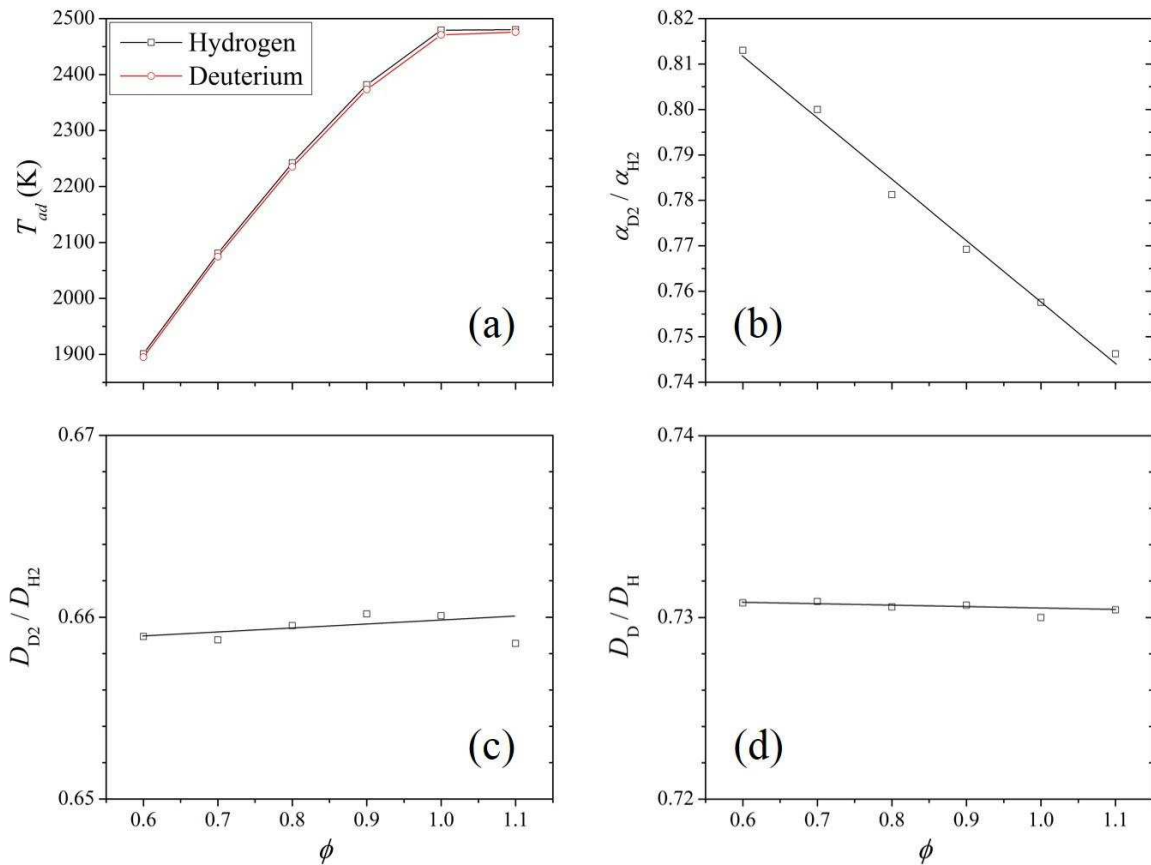
365 Focusing on the results of Figure 8, an increase in burn rate with  $\phi$  was measured for both fuels  
366 over the range of  $\phi$  explored. The ratio  $u_{n,D2} / u_{n,H2}$  varied from  $0.69 \pm 0.05$  at  $\phi = 0.6$  to  $0.73 \pm$   
367  $0.1$  at  $\phi = 1.1$  for both flame radii assessed. These findings are almost identical to those reported  
368 in [19] for hydrogen and deuterium flames with oxygen, albeit this earlier paper did not indicate  
369 whether the flames were cellular.

370 Data reported in [13] for hydrogen-air mixtures are compared with the schlieren derived laminar  
371 burn rates for H<sub>2</sub>-air reported here (Figure 8, top graph). The apparatus and initial conditions used  
372 in the two studies were identical. Differences in the burn rates ranged from  $\sim 1\%$  at  $\phi = 0.6$  to a  
373 maximum of  $\sim 4\%$  at  $\phi = 1.0$ . These small discrepancies could be attributed to uncertainties in the  
374 equivalence ratio and slight differences in the imaging equipment and processing technique used.  
375 In another study of H<sub>2</sub> combustion performed in the Leeds MkII bomb [10], utilisation of a faster  
376 digital camera system enabled the determination of unstretched laminar burning velocities.  
377 Values of  $u_1$  reported in [10] were 30-40% lower compared to the  $u_{n,10mm}$  values presented here,  
378 with the percentage difference becoming smaller with increasing  $\phi$ . Given that there is a very  
379 early transition from laminar to cellular H<sub>2</sub> flames, and especially for lean flames, these  
380 differences could be attributed, primarily, to the effect of cellularity and, secondarily, to the effect  
381 of stretch rate.

382 To enable interpretation of the observed behaviour, computations for  $T_{ad}$  and transport  
383 coefficients were performed using the methods cited in Section 3.1 for the alkanes. In this case,  
384 any additional thermodynamic data required for the calculations was found in [46]. Although the  
385 overall predicted trend in  $T_{ad}$  vs  $\phi$  was consistent with that for the laminar burn rate vs  $\phi$  (cf.  
386 Figure 9a and Figure 8), the differences between the adiabatic flame temperature for H<sub>2</sub> and D<sub>2</sub> at  
387 a given equivalence ratio were too small to account for the measured differences in their laminar



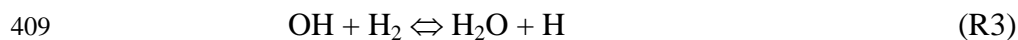
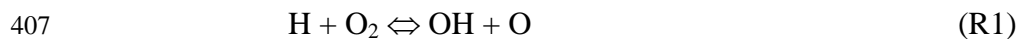
388 burn rates. Also included in Figure 9 are computations for the ratios of thermal diffusivity of the  
 389 mixtures,  $\alpha_{D_2\text{-air}} / \alpha_{H_2\text{-air}}$  (Fig. 9b), and effective mass diffusivities,  $D_{D_2} / D_{H_2}$  (Fig. 9c), and  $D_D /$   
 390  $D_H$  (Fig. 9d), at the constant pressure (0.5 MPa) adiabatic flame temperature. Computed values  
 391 for  $\alpha_{D_2\text{-air}} / \alpha_{H_2\text{-air}}$  ranged between 0.81 at  $\phi = 0.6$  and 0.75 at  $\phi = 1.1$ . Values for the mass  
 392 diffusivities were calculated to be  $D_{D_2} / D_{H_2} \sim 0.66$  and  $D_D / D_H \sim 0.73$  at all equivalence ratios  
 393 explored. The ratios for  $D_{D_2} / D_{H_2}$  given here are consistent with that derived by Gray et al [20],  
 394 for which  $D_{D_2} / D_{H_2} = 0.72$  over a range of burnt gas compositions of  $H_2 - O_2$  and  $D_2 - O_2$  flames  
 395 at low pressure. Based on a dependence of flame speed proportional to  $\sqrt{D}$ , they attributed a  
 396 maximum decrease in flame speed in deuterium-containing mixtures to be 0.85 of that in  
 397 hydrogen-containing mixtures. This is insufficient to account solely for the overall differences  
 398 observed in the burning velocities.



400 Figure 9 – Computed adiabatic temperatures for H<sub>2</sub>-air, D<sub>2</sub>-air flames for initial conditions of 360  
401 K and 0.5 MPa. Also shown are ratios of thermal diffusivities of D<sub>2</sub> over H<sub>2</sub> and mass  
402 diffusivities of D<sub>2</sub> over H<sub>2</sub> and D over H calculated at the constant pressure (0.5 MPa) adiabatic  
403 flame temperature.

404

405 Numerous studies [e.g. 11, 47-48] have highlighted the critical importance of reactions R1 to R4  
406 on controlling the burning velocity of H<sub>2</sub>-air flames.



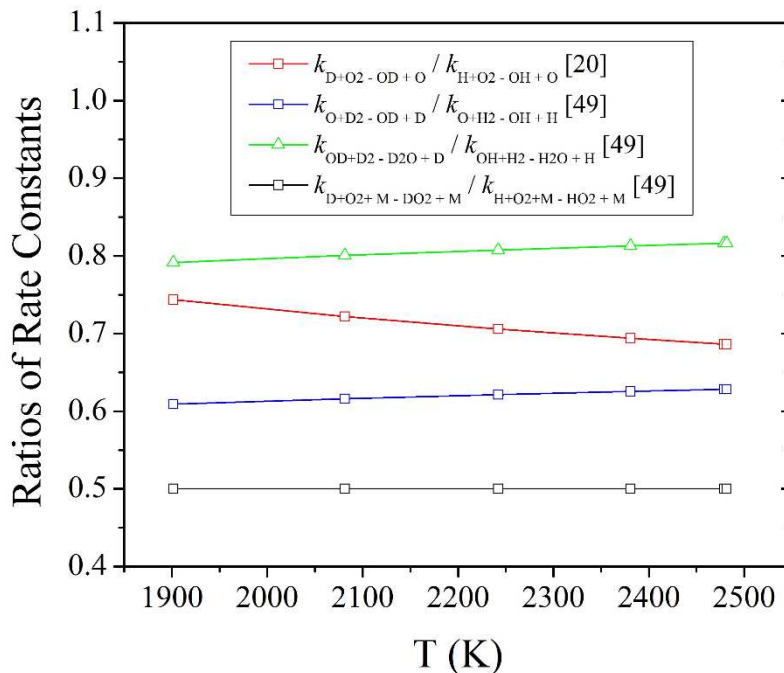
411 The burn rate of the D<sub>2</sub> – air system is similarly controlled by the equivalent reactions. However,  
412 their rates will be susceptible to kinetic isotope effects, which must effect the corresponding rate  
413 constants. The ratios,  $k_D/k_H$ , for the forward Reactions R1 – R4 are displayed in Figure 10. Data  
414 were taken from references [20, 49]. The computations showed that the rate constants of D<sub>2</sub> were  
415 approximately 0.71, 0.62, 0.8 and 0.5 times those of H<sub>2</sub> for reactions R1, R2, R3 and R4,  
416 respectively. An analysis by Gray et al [20] attributed a geometric mean of the ratio of the rate  
417 constants ( $k_D/k_H$ ) for reactions R1 – R3 at 2500K to be 0.59.

418 The dependence of the laminar burning velocity on the fundamental physical and kinetic  
419 parameters has been described as  $u_n \sim (\alpha \cdot \omega)^{0.5}$ , where  $\alpha$  is the thermal diffusivity of the mixture  
420 and  $\omega$  is the global reaction rate [50]. This approximation is likely to be more valid for the  
421 relatively simple H<sub>2</sub>-air and D<sub>2</sub>-air combustion systems, than for those of hydrocarbon fuels. The  
422 laminar burn rate of deuterium could thus be estimated via,

423

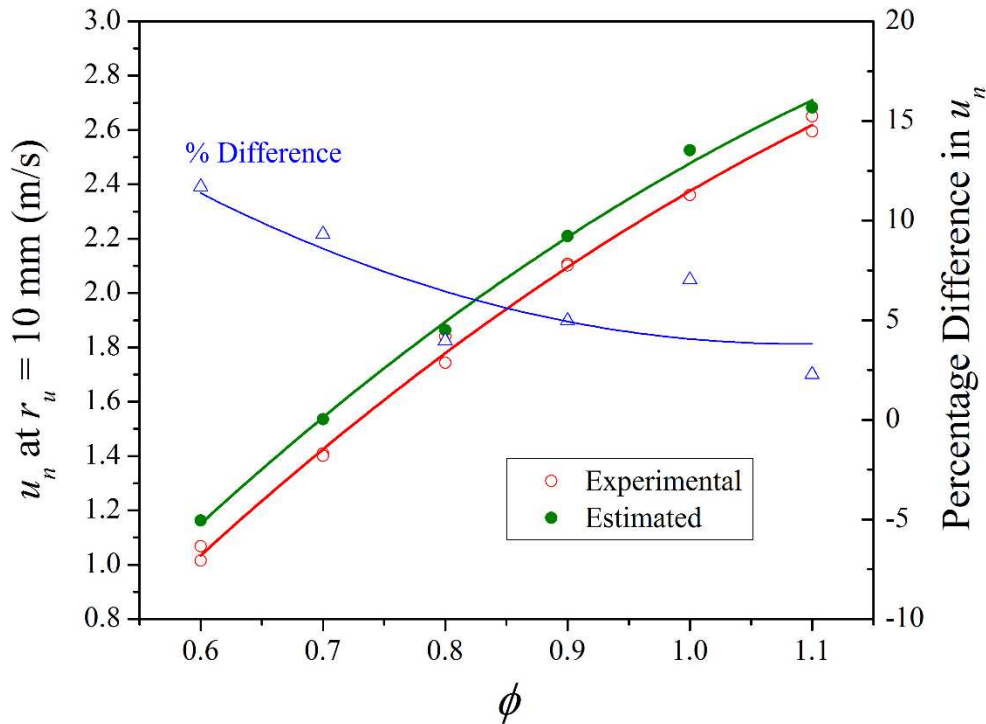
$$u_{n,D2} \sim \left( \frac{(a.\omega)_{D2}}{(a.\omega)_{H2}} \right)^{0.5} \cdot u_{n,H2} \quad (2)$$

424 The reaction rate terms in Eq. (2) were set to be equal to the weighted average of the reaction  
 425 rates of the critically important Reactions R1-R4. This weighted average was based on laminar  
 426 burn rate sensitivity factors,  $S_i$ , reported in [11]. More specifically, to get the global reaction rate  
 427 ratio of Eq. (2), the  $k_D/k_H$  ratios for reactions R1 – R4 (Figure 10) were multiplied by weighted  
 428 laminar burn rate sensitivity factors, determined as  $S_{i,w} = S_i / \sum S_i$ . The values used for the thermal  
 429 diffusivity ratio of equation 2 were those displayed in Figure 9b. The  $u_{n,D2}$  values estimated via  
 430 equation 2, combined with experimental  $u_{n,H2}$  data, are shown in Figure 11. Agreement with the  
 431 experimentally measured laminar burn rates of D<sub>2</sub>-air flames is good. The difference ranged from  
 432 ca. 12% at  $\phi = 0.6$  to ca. 2% at  $\phi = 1.1$ . The over-prediction at lean mixtures could be attributed  
 433 to the effects of cellularity, encapsulated in the experimentally determined  $u_{n,H2}$  data used for the  
 434 estimate. The reasoning behind this was described at the beginning of this section, with respect to  
 435 the discussion of the results of Figure 8.



436

437 Figure 10 – Ratios of selected reaction rate constants,  $k_{D_2} / k_{H_2}$ , at temperatures relating to the  $T_{ad}$   
 438 at each of the equivalence ratios for which burn rates were experimentally measured.

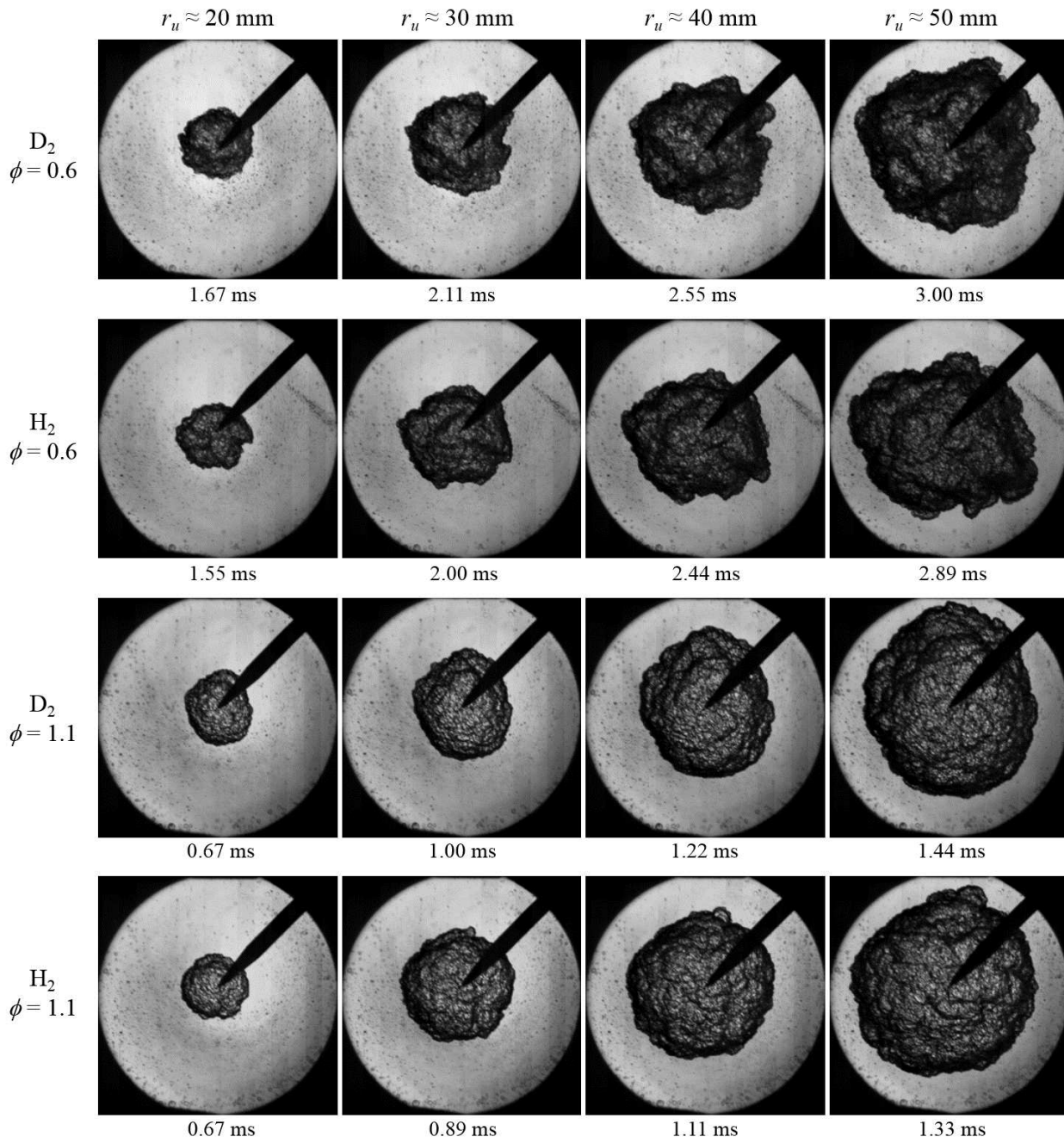


439  
 440 Figure 11 – Comparison between measured and estimated burn rates of  $D_2$ -air laminar flames at  
 441 various equivalence ratios. The curves are 2<sup>nd</sup> order polynomial fits of the data, added for better  
 442 illustration.

443  
 444 **3.4 Turbulent Burning Velocities of  $H_2$  and  $D_2$  flames in air**

445 For completeness, a filmstrip showing  $H_2$ -air and  $D_2$ -air flame images for the leanest and richest  
 446 conditions explored in this study is included in Figure 12. For both fuels, lean flames appeared  
 447 more distorted compared to rich flames. Schlieren derived turbulent burning velocities for  $H_2$  and  
 448  $D_2$  at mean flame radii of 30 mm and  $u' = 4$  m/s, over the range  $\phi = 0.6$  to  $\phi = 1.1$ , are displayed  
 449 in Figure 13. To indicate the experimental scatter, also included in Figure 13 is the standard  
 450 deviation from the average  $u_{te}$  values at each condition. The change from laminar to turbulent

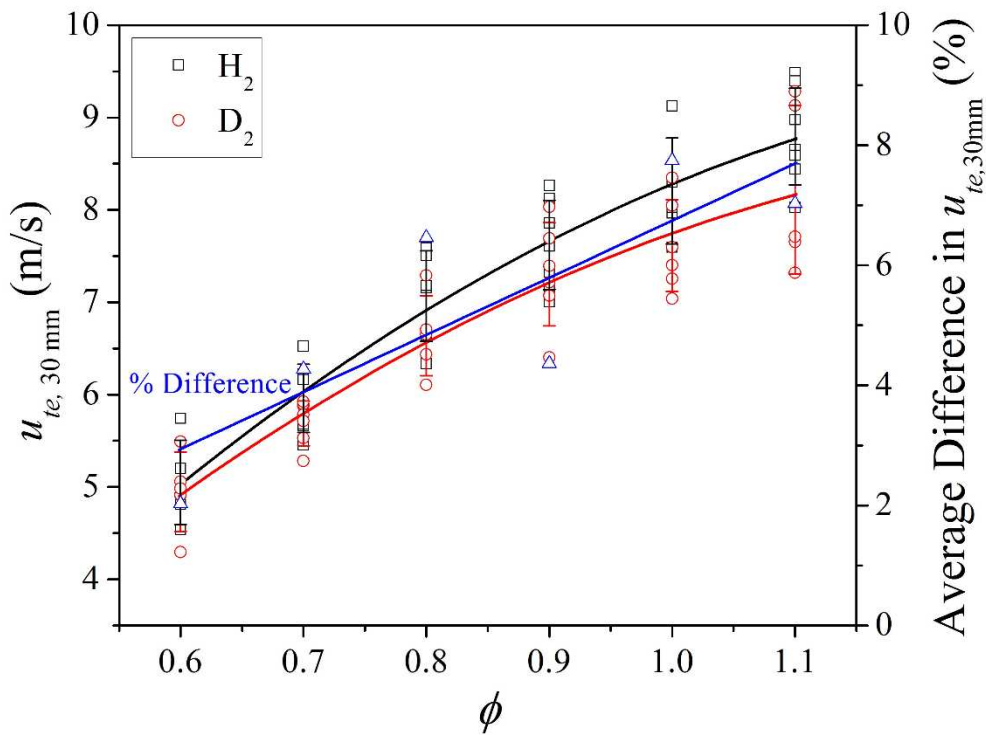
451 conditions resulted in a significant reduction in the burn rate differences between H<sub>2</sub> and D<sub>2</sub>.  
452 These differences fell from 25-30% under laminar conditions to ~ 5% when turbulence was  
453 present. This reduction was more marked than that for the normal vs deuterated alkanes, as  
454 discussed in Section 3.2.



456 Figure 12 – Filmstrips of turbulent flame images for H<sub>2</sub> and D<sub>2</sub> at equivalence ratios of 0.6 and  
 457 1.1. The mean flame radius values indicated have minimum accuracy of ± 1.0 mm.

458

459 Although a general trend to lower turbulent burning velocities of D<sub>2</sub> flames relative to those of H<sub>2</sub>  
 460 is evident in Figure 12, the individual results tend to overlap within the range of experimental  
 461 scatter. The similarity between the turbulent burning velocities of deuterium and hydrogen  
 462 flames, contrasted with the marked difference of their laminar burning velocities, suggests that  
 463 turbulent transport processes have a greater influence on the flame propagation rate than kinetic  
 464 isotope effects involved in the kinetic chain branching reactions.



465

466 Figure 13 – Schlieren based turbulent burning velocities ( $u' = 4$  m/s) for hydrogen and deuterium  
 467 at a mean flame radius of 30 mm. The standard deviation from average experimental data at each  
 468 condition along with the average percentage difference between the two fuels are also shown.

469

470 Application of Eq. (1) for the H<sub>2</sub> and D<sub>2</sub> flames examined is not as straightforward as for the  
471 normal and deuterated alkanes. First, for reasons discussed earlier in Section 3.3, the analysis for  
472 the H<sub>2</sub> and D<sub>2</sub> laminar flames could not yield a true unstretched laminar burning velocity, as  
473 required for appropriate application of Eq. (1). Second, owing to their very high laminar burn rate  
474 and small flame thickness, the H<sub>2</sub> and D<sub>2</sub> turbulent flames examined are classified as corrugated  
475 flames, in which case the condition of  $\eta \ll \delta_1$  does not necessarily stand. Nonetheless,  
476 estimations made through Eq. (1) still are in fair agreement with the experiments. Estimations  
477 from Eq. (1) for the  $u_{te}$  ratio between D<sub>2</sub> and H<sub>2</sub> ranged from 0.88 at lean conditions to 0.94 at  
478 rich conditions.

479

#### 480 **4. Conclusions**

481 Substitution of the hydrogen atoms in n-hexane and n-octane with deuterium atoms resulted in a  
482 reduction of ca. 20% in the measured laminar burning velocity, despite there being little  
483 difference in molar mass or calculated adiabatic flame temperatures, and no expectation of  
484 qualitative differences in the kinetic scheme for full oxidation of the normal and deuterated  
485 alkane counterparts. Also, it was assumed that the kinetic scheme for full oxidation of the normal  
486 and deuterated alkane counterparts were the same. The normal alkane flames were observed to  
487 become cellular slightly earlier. Nonetheless, insofar that comparisons were made with respect to  
488 the unstretched burning velocities calculated using data corresponding to the pre-cellular region  
489 of the flame, instability effects cannot be considered to be significant. It is concluded that the  
490 observed difference in laminar burn rates between normal and deuterated n-hexane and n-octane  
491 are the result, predominantly, of the higher thermo-diffusivity and reactivity of hydrogen atoms  
492 relative to those of deuterium atoms.

493 Measured laminar burn rates for H<sub>2</sub>-air flames were 30% higher than for D<sub>2</sub>-air flames, at fixed  
494 ambient temperature, pressure and equivalence ratios. This difference was also linked to the  
495 thermo-diffusive and chemical kinetic properties of H vs D atoms. The ratios of thermal and mass  
496 diffusivity of deuterium over hydrogen atoms, as well as corresponding reaction rate ratios for the  
497 important chain branching reactions involving D and H, were estimated to be within 0.6 – 0.8  
498 over the range of conditions explored, which is very similar to the measured difference in laminar  
499 burn rate. The higher laminar burn rate difference between H<sub>2</sub> and D<sub>2</sub> compared with that  
500 measured for normal versus deuterated alkanes would be expected, in view of the kinetic  
501 complexity and weakened isotope effect in the hydrocarbon combustion chemistry.

502 Under turbulent conditions, differences in the burn rate between normal and deuterated n-hexane  
503 and n-octane were much smaller, with the deuterated alkanes being ~8% slower than their normal  
504 counterparts. It is concluded that turbulence globally accelerates species diffusivity, rendering  
505 transport properties of species within the preheat zone more important for turbulent compared to  
506 laminar flames. Given that the thermal diffusivity of the parent fuels is almost identical between  
507 the normal and deuterated alkane counterparts, the residual influence of kinetic isotope effects is  
508 expressed as  $u_1^{0.5}$ .

509 The difference between the burn rates of H<sub>2</sub>-air flames and D<sub>2</sub>-air flames under turbulence was  
510 reduced by a factor of five relative to that observed under laminar conditions. These findings  
511 emphasise that transport properties, globally boosted by turbulent diffusivity, exert greater  
512 control than kinetic isotope effects during turbulent combustion. The measured turbulent burning  
513 velocity ratios at each mixture stoichiometry examined were adequately replicated via application  
514 of the Zimont submodel for turbulent burning velocity, defined in Eq. (1).

515



516 **Acknowledgements**

517 The support of Exxon Mobil and Mercedes-Benz High Performance Engines is gratefully  
518 acknowledged.

519

520 **References**

- 521 [1] Gu, X., Huang, Z., Wu, S., “Laminar burning velocities and flame instabilities of butanol  
522 isomers–air mixtures”, *Combust Flame* 157: 2318-2325 (2010)
- 523 [2] Wu, F., Kelley, A.P., Law, C.K., “Laminar flame speeds of cyclohexane and mono-  
524 alkylated cyclohexanes at elevated pressures”, *Combust Flame* 159: 1417-1425 (2012)
- 525 [3] Mehl, M., Herbinet, O., Dirrenberger, P., Bounaceur, R., Glaude, P.A., Battin-Leclerc, F.,  
526 Pitz, W.J., “Experimental and modeling study of burning velocities for alkyl aromatic  
527 components relevant to diesel fuels”, *Proc Combust Inst* 35: 341-348 (2015)
- 528 [4] Farrell, J.T., Johnston, R.J., Androulakis, I.P., “Molecular Structure Effects on Laminar  
529 Burning Velocities at Elevated Temperature and Pressure”, *SAE Tech Paper* 2004-01-  
530 2936 (2004)
- 531 [5] Beeckmann, J., Cai, L., Pitsch, H., “Experimental investigation of the laminar burning  
532 velocities of methanol, ethanol, n-propanol and n-butanol at high pressure”, *Fuel* 117:  
533 340-350 (2014)
- 534 [6] Burluka, A.A., Gaughan, R.G., Griffiths, J.F., Mandilas, C., Sheppard, C.G.W., Woolley,  
535 R., “Turbulent burning rates of gasoline components, Part 1 – Effect of fuel structure of  
536 C6 hydrocarbons”, *Fuel* 167: 347-356 (2016)

- 537 [7] Burluka, A.A., Gaughan, R.G., Griffiths, J.F., Mandilas, C., Sheppard, C.G.W., Woolley,  
538 R., "Turbulent burning rates of gasoline components, Part 2 – Effect of carbon number",  
539 Fuel 167: 357-365 (2015)
- 540 [8] Friedman, R., Burke, E., "Burning Velocities. Acetylene and Dideutero-Acetylene with  
541 Air", Ind Eng Chem 43: 2772-2776 (1951)
- 542 [9] Buttini, P., Corno, C., Latella, A., Prastaro, M., "Relevance of adding deuterated  
543 hydrocarbons to fuels in the automotive emissions studies", SAE Paper 982622, 1998
- 544 [10] Bradley, D., Lawes, M., Liu, K., Verhelst, S., Woolley, R., "Laminar burning velocities of  
545 lean hydrogen–air mixtures at pressures up to 1.0 MPa", Combust Flame 149: 162-172  
546 (2007)
- 547 [11] Hu, E., Huang, Z., He, J., Miao, H., "Experimental and numerical study on laminar  
548 burning velocities and flame instabilities of hydrogen-air mixtures at elevated pressures  
549 and temperatures", Int J Hydrogen Energ 34: 8741-8755 (2009)
- 550 [12] Pareja, J., Burbano, H.J., Amell, A., Carvajal, J., "Laminar burning velocities and flame  
551 stability analysis of hydrogen/air premixed flames at low pressure" Int J Hydrogen Energ  
552 36: 6317-6324 (2011)
- 553 [13] Verhelst, S., Woolley, R., Lawes, M., Sierens, R., "Laminar and Unstable Burning  
554 Velocities and Markstein Lengths of Hydrogen–Air Mixtures at Engine-Like Conditions",  
555 Proc Combust Inst, 30: 209-216 (2005)
- 556 [14] Zamashchikov, V.V., Alekseev, V.A., Konnov, A.A., "Laminar burning velocities of rich  
557 near-limiting flames of hydrogen", Int J Hydrogen Energ 39: 1874-1881 (2014)
- 558 [15] Dahoe, A.E., "Laminar burning velocities of hydrogen–air mixtures from closed vessel  
559 gas explosions", Journal of Loss Prevention in the Process Industries, 18: 152-166 (2005)

- 560 [16] Kido, H., Nakahara, M., Nakashima, K., and Kim, J., "Turbulent Burning Velocity of  
561 Lean Hydrogen Mixtures", SAE Technical Paper 2003-01-1773 (2003)
- 562 [17] Kitagawa, T., Nakahara, T., Maruyana, K., Kado, K., Hayakawa, A., Kobayashi, S.,  
563 "Turbulent burning velocity of hydrogen–air premixed propagating flames at elevated  
564 pressures", Int J Hydrogen Energ 33: 5842-5849 (2008)
- 565 [18] Amato, A., Day, M., Cheng, R.K., Bell, J., Dasgupta, D., Lieuwen, T., "Topology and  
566 burning rates of turbulent, lean, H<sub>2</sub>/air flames", Combust Flame 162: (2015) 4553-4565
- 567 [19] Gray, P., Smith, D.B., "Isotope effects on flame speeds for hydrogen and deuterium",  
568 Chem Commun (London) 146-148 (1967)
- 569 [20] Gray, P., Holland, S., Smith, D.B., "The effect of isotopic substitution on the flame speeds  
570 of hydrogen-oxygen and hydrogen-nitrous oxide flames", Combust Flame 14: 361-374  
571 (1970)
- 572 [21] Koroll, G.W., Kumar, R.K., "Isotope effects on the combustion properties of deuterium  
573 and hydrogen, Combust Flame 84: 154-159 (1991)
- 574 [22] Gillespie, L., Lawes, M., Sheppard, G.G.W., Woolley, R., "Aspects of Laminar and  
575 Turbulent Burning Velocity Relevant to SI Engines", SAE Tech Paper 2000-01-0192  
576 (2000)
- 577 [23] Heywood, J.B., "Internal Combustion Engine Fundamentals, International Edition", Mc  
578 Graw Hill, ISBN 0071004998 (1988)
- 579 [24] Mandilas, C., "Laminar and Turbulent Burning Characteristics of Hydrocarbon Fuels",  
580 PhD Thesis, University of Leeds (2008)

- 581 [25] Bradley, D., Gaskel, P.H., Gu, X.J., “Burning Velocities, Markstein Length, and Flame  
582 Quenching for Spherical Methane-Air Flames: A Computational Study”, *Combust Flame*  
583 104: 176-198 (1996)
- 584 [26] Bradley, D., Hicks, R.A., Lawes, M., Sheppard, C.G.W., Woolley, R., “The Measurement  
585 of Laminar Burning Velocities and Markstein Numbers for Iso-octane–Air and Iso-  
586 octane–n-Heptane–Air Mixtures at Elevated Temperatures and Pressures in an Explosion  
587 Bomb”, *Combust Flame* 115: 126-144 (1998)
- 588 [27] Lamoureux, N., Djebaili-Chaumeix, N., Paillard, C.E., “Laminar flame velocity  
589 determination for H<sub>2</sub>–air–He–CO<sub>2</sub> mixtures using the spherical bomb method”, 2nd  
590 Mediterranean Comb Symp, *Exp Therm Fluid Sci* 27: 385-393 (2003)
- 591 [28] Jerzembeck, S., Peters, N., “Laminar Spherical Flame Kernel Investigation of Very Rich  
592 Premixed Hydrocarbon-Air Mixtures in a Closed Vessel under Microgravity Conditions”,  
593 SAE Tech Paper 2008-01-0471 (2008)
- 594 [29] Chen, Z., Wei, L., Huang, Z., Miao, H., Wang, X., Jiang, D., “Measurement of Laminar  
595 Burning Velocities of Dimethyl Ether–Air Premixed Mixtures with N<sub>2</sub> and CO<sub>2</sub>  
596 Dilution”, *Energ Fuels*, 23: 735-739 (2009)
- 597 [30] Varea, E., Modica, V., Vandel, A., Renou, B., “Measurement of laminar burning velocity  
598 and Markstein length relative to fresh gases using a new post-processing procedure.  
599 Application to laminar spherical flames for methane, ethanol and isooctane/air mixtures”,  
600 *Combust Flame* 159: 577-590 (2012)
- 601 [31] Moghaddas, A., Eisazadeh-Far, K., Metghalchi, H., “Laminar burning speed measurement  
602 of premixed n-decane/air mixtures using spherically expanding flames at high  
603 temperatures and pressures”, *Combust Flame* 159: 1437-1443 (2012)

- 604 [32] Lawes, M., Ormsby, M.P., Sheppard, C.G.W., Woolley, R., “Variation of Turbulent  
605 Burning Rate of Methane, Methanol and Isooctane Air Mixtures with Equivalence Ratio  
606 at Elevated Pressure”, *Combust Sci Technol* 177: 1273-1289 (2005)
- 607 [33] Abdi Aghdam, E., Burluka, A.A., Hattrell, T., Liu, K., Sheppard, C.G.W., Neumeister, J.  
608 and Crundwell, N., “Study of Cyclic Variation in an SI Engine using Quasi-Dimensional  
609 Combustion Model”, *SAE Paper* 2007-01-0939 (2007)
- 610 [34] Law, C.K., “Dynamics of Stretched Flames”, *22nd Symp Int Combust* 22: 1381-1402  
611 (1988)
- 612 [35] Bradley, D., Sheppard, C.G.W., Woolley, R., Greenhalgh, D.A., Lockett, R.D., “The  
613 development and structure of flame instabilities and cellularity at low Markstein numbers  
614 in explosions”, *Combust Flame* 122: 195-209 (2000)
- 615 [36] Bradley, D., Lung, F.K., Spark ignition and the early stages of turbulent flame  
616 propagation, *Combust Flame* 69: 71-93 (1987)
- 617 [37] Abdel-Gayed, R.G., Bradley, D., Lawes, M., “Turbulent burning velocities: a general  
618 correlation in terms of straining rates”, *Proc R Soc Lond A*414: 389-413 (1987)
- 619 [38] Jomaas, G., Law, C.K., Bechtold, J.K., On transition to cellularity in expanding spherical  
620 flames, *J Fluid Mech*, 583: 1-26 (2007)
- 621 [39] Bird, R.B., Stewart, W.E., Lightfoot, E.N., “Transport Phenomena, 2nd Edition”, Wiley &  
622 Sons, ISBN 0471410772 (2002)
- 623 [40] Wilke, C.R., “A viscosity equation for gas mixtures”, *J Chem Phys* 18: 517-519 (1950)
- 624 [41] Gaughan, R., Private Communication, University of Leeds (2008)
- 625 [42] <http://webbook.nist.gov/chemistry/>, accessed 05/2016
- 626 [43] Borghi, R., “Turbulent combustion modeling”, *Prog Ener Comb* 14: 245-292 (1988)

- 627 [44] Zimont, V.L. “To computations of turbulent combustion of partially premixed gases,  
628 chemical physics of combustion and explosion processes. Combustion of multi-phase and  
629 gas systems”, OIKhF, Chernogolovka (1977) p. 77–80 (in Russian)
- 630 [45] Lipatnikov, A.N., Chomiak, J., “Turbulent flame speed and thickness: phenomenology,  
631 evaluation, and application in multi-dimensional simulations”, Prog Energ Comb Sci, 28:  
632 1-74 (2002)
- 633 [46] <http://garfield.chem.elte.hu/Burcat/burcat.html>, accessed 05/2016
- 634 [47] Marinov, N.M., Curran, H.J., Pitz, W.J., Westbrook, C.K., “Chemical Kinetic Modeling  
635 of Hydrogen under Conditions Found in Internal Combustion Engines”, Energ Fuels 12:  
636 78–82 (1998)
- 637 [48] Dong, Y., Holley, A.T., Andac, M.G., Egolfopoulos, F.N., Davis, S.G., Middha, P., Wang,  
638 H., “Extinction of premixed H<sub>2</sub>/air flames: Chemical kinetics and molecular diffusion  
639 effects”, Combust Flame 142: 374-387 (2005)
- 640 [49] Pamidimukkala, K.M., Skinner, G.B., “Resonance absorption measurements of atom  
641 concentrations in reacting gas mixtures. VIII. Rate constants for O+H<sub>2</sub>→OH+H and  
642 O+D<sub>2</sub>→OD+D from measurements of O atoms in oxidation of H<sub>2</sub> and D<sub>2</sub> by N<sub>2</sub>O”, J.  
643 Chem Phys 76: 311-315 (1982)
- 644 [50] Glassman, I., “Combustion, 3rd Edition”, Academic Press, ISBN 0122858522 (1996)